VI. Conclusion

Information has been given for the utilization of reactive microstrip circuit elements: the radial-line stub, a microstripline loop paralleling a series reactance, and coupled microstrip stubs. With the exception of the radial-line stub, these components have been treated as two-port elements in parallel connection with a lumped impedance, assumed to be connected in series with the microstripline. Specifically, the element parameters have been derived for the case in which the combination of reactive element and lumped impedance effectively form a blocking filter at the design frequency. This configuration is that required for high isolation in the design of a microstrip switch using a switchable semiconductor element in series with the line.

References

[1] J. P. Vinding, "Radial line stubs as elements in stripline circuits," *NEREM. Record*, pp. 108–109, 1967.

[2] *Broadband microstrip mixer design: The Butterfly Mixer*, Hewlett-Packard, App. note no. 976, 1980.

[3] W. V. McLevige and V. Sokolov, "Microwave switching with parallel-resonated GaAs FET's," *Electron Devices Lett.*, vol. EDL-1, pp. 155–158, Aug. 1980.

[4] V. McLevige and V. Sokolov, "Resonated GaAs FET devices for microwave switching," *IEEE Trans. Electron Devices*, vol. ED-28, pp. 198–204, Feb. 1981.

[5] G. I. Zysman and A. K. Johnson, "Coupled-line transmission networks in an inhomogeneous dielectric medium," *IEEE Trans. Microwave Theory Tech.*, vol. MTT-17, pp. 753–759, Oct. 1969.

[6] T. G. Bryant and J. A. Weiss, "Parameters of microstrip transmission lines and of coupled pairs of lines," *IEEE Trans. Microwave Theory Tech.*, vol. MTT-16, pp. 1021–1027, Dec. 1968.

[7] T. G. Bryant and J. A. Weiss, "MSTRIP (Parameters of microstrip)," *IEEE Trans. Microwave Theory Tech.*, vol. MTT-19, p. 418, Apr. 1971.

[8] R. Garg and I. J. Bahl, "Characteristics of coupled microstriplines," *IEEE Trans. Microwave Theory Tech.*, vol. MTT-27, pp. 700–705, July 1979.

[9] K. C. Gupta *et al.*, *Computer-Aided Design of Microwave Circuits*. Dedham, MA: Artech House, 1981, sec. 3.8.

An Optimized *L*-Band Eight-Way Gysel Power Divider–Combiner

FIORENZO ARDEMAGNI, MEMBER, IEEE

Abstract—**Theoretical analysis of a general *n*-way power divider-combiner in a Gysel configuration has been carried out to derive relationships among fundamental parameters. On the basis of its symmetries, an eight-way network has been described, analyzed, and optimized over a 25-percent bandwidth by the computer program COMPACT™.**

Experimental data is reported and compared with theoretical predictions.

I. Introduction

The most popular *n*-way in-phase power divider–combiner (PDC) was proposed by Wilkinson in 1960 [1]. With the advent of microwave integrated circuits (MIC's) in the late 1960's it was immediately clear that, for $n > 2$, this kind of network is impractical to develop due to the nonplanarity introduced by the internal resistor star. Furthermore, as was pointed out by many authors [2], [3], the internal resistors are not connected to ground, so that heat-sinking and tuning of parasitic capacitances is difficult to achieve.

Gysel introduced in 1975 a modification of the concept [3] which from the practical standpoint has proven until now to be more suitable than others for high-power applications. In fact, the inconveniences presented by the Wilkinson topology are overcome.

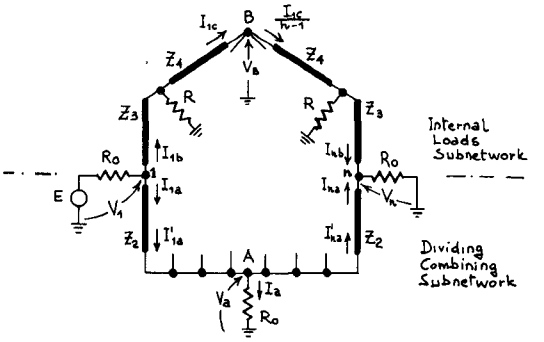

Fig. 1. *n*-way Gysel PDC.

As it will be shown later, although it is not realizable in a single plane for $n > 2$ in the same way as its forefather, the Gysel structure lends itself to being easily realized in microstrip or stripline also, for moderately high *n*.

In spite of that, the use of Gysel PDC has not become widespread, probably due to the lack of theoretical analysis on the subject and the complexity of optimizing the network on medium-to-wide bandwidth for an increasing splitting factor *n*.

In this paper it is intended to clarify some points of the matter, introducing at the same time an approach to eliminate node limitations of the program COMPACT™. The methodology is then applied to the practical case of an eight-way PDC designed for solid-state transmitters in the 960–1215-MHz Navaids frequency range (DME or TACAN).

II. Theoretical Analysis

To derive the exact relationship for the Gysel configuration, we can follow the same reasoning adopted by Wilkinson [1]. Let us consider Fig. 1 with all lines a quarter-wavelength long.

Then

$$V_1 = jI'_{1a}Z_2$$

$$I_{1a} = j\frac{V_a}{Z_2} \tag{1}$$

$$V_a = jI_{na}Z_2$$

$$I'_{na} = j\frac{V_n}{Z_2}. \tag{2}$$

On the other hand, since all branches are identical, we have

$$I'_{1a} = \frac{V_a}{Ro} - (n-1)I'_{na} \tag{3}$$

and it is also true that

$$I_{na} = \frac{Vn}{Ro} = I_{nb} \qquad I_{1a} = \frac{E - V_1}{Ro} - I_{1b}. \tag{4}$$

Combining (1)–(4), we can eliminate the currents (see Appendix) leaving the system of the three unknowns V_a, V_1, and V_n

$$V_1 = jV_a\frac{Z_2}{Ro} + (n-1)V_n$$

$$V_a = jV_n\frac{Z_2}{Ro} - jZ_2\frac{R}{nZ_3^2}(V_1 - V_n)$$

$$\frac{E - V_1}{Ro} = j\frac{Va}{Z_2} + \frac{n-1}{n}\frac{R}{Z_3^2}(V_1 - V_n). \tag{5}$$

Manuscript received June 11, 1982; revised February 7, 1983.

The author is with LCF—Industrie Face Standard S.P.A., Via della Magione, 10, 00040 Pomezia, Italy.

0018-9480/83/0600-0491$01.00 ©1983 IEEE

```
100 TRL AA SE -50 90 1000
200 TRL BB SE -141.42 90 1000
300 TRL PP SE -50 90 1000
400 RES QQ PA 50
500 TRL RR SE -17.68 90 1000
600 RES TT SE 50
610 CAX PP RR
620 CON PP T2 2 6
630 CON PP T2 3 6
640 CON PP T2 4 6
650 CON PP T2 5 6
660 CON BB T2 1 2
670 CON BB T2 1 3
680 CON BB T2 1 4
690 CON BB T2 1 5
700 CON TT T2 3 0
710 CON TT T2 4 0
720 CON TT T2 5 0
730 DEF B1 T3 1 2 6
740 CON B1 T3 1 2 3
750 CON B1 T3 1 4 3
760 CON TT T2 4 0
770 DEF KK T2 1 2
780 CAS AA KK
790 PRI AA S1 50
800 END
810 1000 1500 50
820 END
830 .05
840 1 1 1 -9.5 GT
850 END
```

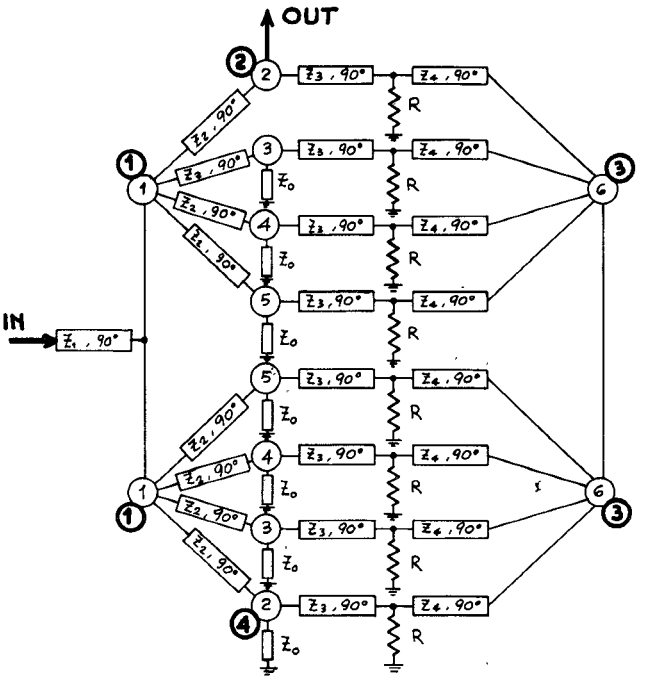

Fig. 2. COMPACT™ data file for transmission loss analysis and optimization of the eight-way Gysel PDC. Light and heavy circles represent first and second hierarchy nodes in the data file, respectively.

For perfect isolation

$$V_n = 0. \tag{6}$$

For perfect match at the input port

$$E = 2V_1. \tag{7}$$

Substituting (6) and (7) into (5) the two fundamental conditions are derived (see Appendix)

$$Z_2 = \sqrt{n}\,Ro \tag{8}$$

$$Z_3 = \sqrt{RRo}\,. \tag{9}$$

As shown in (8) and (9), the isolation and the matching of all ports is independent of Z_4 at midband. In order to verify how the arbitrary parameter Z_4 affects the behavior of the network over frequency, a two-way PDC has been analyzed using the computer porgram COMPACT™ [4].

The results have demonstrated that a value of Z_4 that simultaneously optimizes all the four PDC relevant quantities (i.e., transmission loss, common port return loss, output ports return loss, and isolation between output ports) does not exist. In particular, transmission loss and common port return loss seem to have the same tendency with respect to this parameter; lower values of Z_4 results in wider bandwidth. The output port isolation is scarcely influenced by the value of Z_4, while output port return loss tends to settle on an acceptably low but flat value over a wide bandwith as Z_4 increases. Then, the designer can select from time to time the more convenient compromise for Z_4, instead of adopting the prevailing custom of putting $Z_4 = Z_0/\sqrt{n}$ [5].

The power dissipated in the internal loads, under the conditions of perfect isolation and match, can be derived with a tedious but easy computation.

We found

$$P_{dj} = \left(\frac{n-1}{n}\right)^2 P_{jav} \tag{10}$$

$$P_{dk} = \frac{1}{n^2} P_{jav}, \qquad j \neq k \tag{11}$$

where P_{dj} is the power dissipated in the internal resistor R_j with available power P_{jav} entering on the same jth port, while P_{dk} is the power in the resistors of the other branches. The power flow to the external load at the common port is

$$P_{out} = \frac{1}{n} P_{jav} \tag{12}$$

so that the identity is verified

$$P_{out} + P_{dj} + (n-1)P_{dk} = P_{jav}. \tag{13}$$

III. EIGHT-WAY PDC

The analysis and optimization of an eight-way structure over a 23.4-percent bandwidth represents an extremely difficult task without the help of a computer program, yet can be afforded at reasonable cost by COMPACT™. The symmetries of the network overcome, by a proper use of the instruction set, the intrinsic limitation of 15 nodes as a maximum and, in principle, any n can be dealt with.

Since the program cannot consider more than two ports, two data files must be set up in order to analyze all four PDC quantities.

From the first one, shown in Fig. 2, transmission loss and matching of the common and the output ports can be derived. The second, essentially the same with the input port and port ④ exchanged, provides data for isolation and, again, the output port matching. There is no way to simultaneously optimize the four parameters; the designer will choose according to his needs which file to submit to optimization and afterwards will use the optimized data for an analysis with the other file.

Starting from the initial "Standard" parameter set

$$Z_1 = 50\ \Omega$$

$$Z_2 = \sqrt{8} \cdot 50 = 141.42\ \Omega$$

$$Z_3 = 50\ \Omega$$

$$Z_4 = 50/\sqrt{8} = 17.68\ \Omega$$

$$R = 50\ \Omega \tag{14}$$

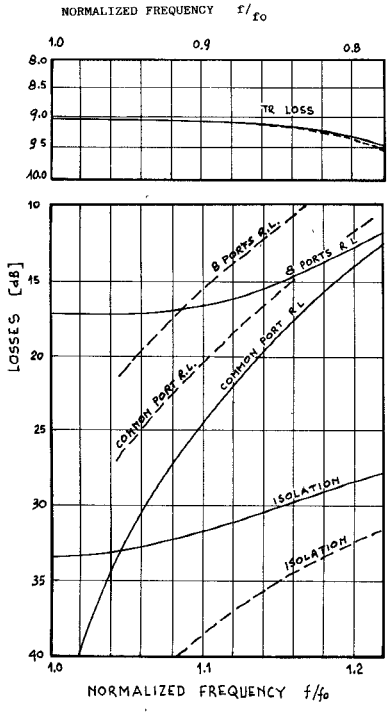

Fig. 3. Behavior of the eight-way Gysel PDC in the "Standard" (dashed) and optimized (full line) configurations.

the optimization of the four characteristic impedances has taken place over the bandwidth $0.78 < f/fo < 1.22$[1] asking for a transmission loss better than 9.5 dB (9.03 dB is the theoretical attenuation at the center frequency for an eight-way divider). Results are reported in Fig. 3 and the final set of optimized variables is

$$Z_1 = 43.19\ \Omega$$
$$A_2 = 123.64\ \Omega$$
$$Z_3 = 42.61\ \Omega$$
$$Z_4 = 20.46\ \Omega$$
$$R = 50\ \Omega \text{ (not optimized)}. \qquad (15)$$

It is interesting to note that Z_2 has been lowered and Z_4 increased by the optimization process, so that they now become realizable for a practical MIC implementation.

Comparison between final set (15) and initial set (14) COMPACT™ analysis shows that over the bandwidth of interest, the matching of all ports has been increased to a value better than 11.7-dB return loss ($\Gamma = 0.26$), against the previously unacceptable value of 7.6 dB of the output ports (at $f/fo = 1.22$). At the same time, the isolation gets worse, but maintains better than 27.7 dB.

The transmission loss decreases from 9.52 dB to 9.45 (at $f/fo = 1.22$) with an improvement of 0.07 dB.

IV. Experimental Results

The eight-way PDC has been realized with two microstrip networks, each one related to the PDC subnetworks shown in Fig. 1, placed at opposite sides of a double-box circular package. Connections between the two sides were performed by coaxial throughs a few millimeters long.

Two different dielectric constant substrates have been used in order to equalize as far as possible the physical length of Z_2 with that of Z_3 and Z_4 together, so that high symmetry and linearity of the structure can be achieved with minimum parasitic reactances. For improved cooling purposes, the internal load resistors are replaced by external ones connected by 50-Ω lines.

In Figs. 4, 5, and 6, some of the measured quantities are

[1]Note: This respresents a wider range (~ 44 percent) than the used bandwidth (~ 23.5 percent).

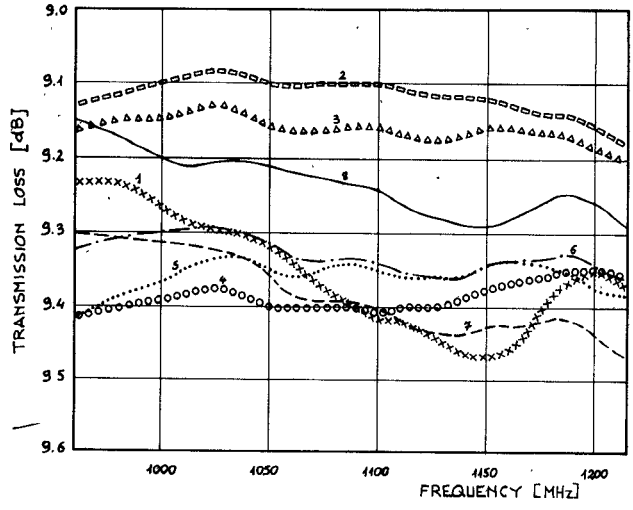

Fig. 4. Eight-way Gysel PDC transmission loss.

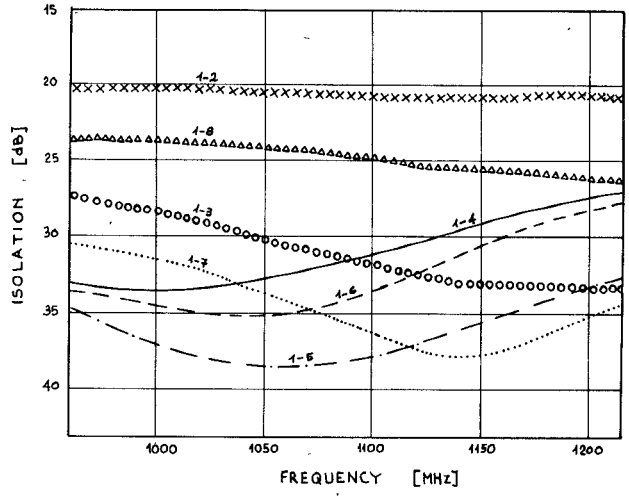

Fig. 5. Eight-way Gysel PDC isolation with respect to port 1.

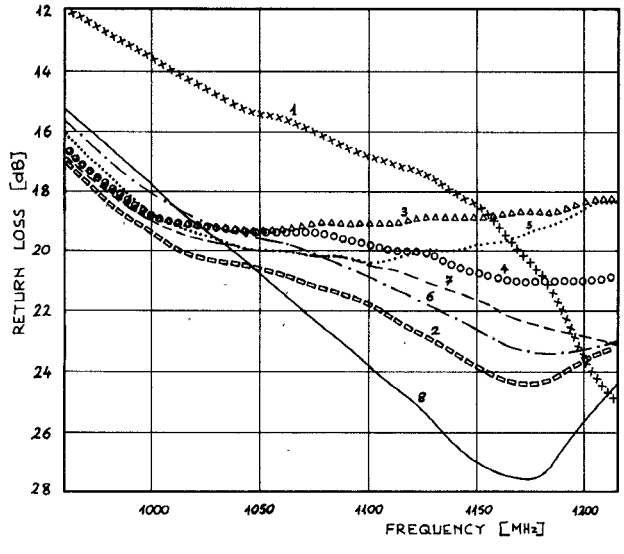

Fig. 6. Eight-way Gysel PDC output ports return loss.

shown. For simplicity, only the isolation with respect to the output port 1 is shown where the worst case of 20 dB appears; for the other 21 possible combinations, the minimum measured values is 22 dB.

The experimental data for the matching of the output ports is in good agreement with the theoretical data at the upper band-edge, but about 4-dB worse at the lower, at least for port 1.

In spite of its, for practical purposes, acceptable value of 22-dB minimum, the common port matching seems to be affected by internal multiple reflections, probably due to uncompensated reactances introduced by the input node A. In attempting to correct this discrepancy, an additional investigation is being carried out at the moment in order to determine the best pattern for the stars of lines at the input node A and the common node B.

The transmission loss data for the experimental PDC shows that all ports are balanced better than ± 0.2 dB over the bandwidth. Compared with the theoretical curve, approximately 0.3-dB fixed dissipation must be taken into account.

V. Conclusions

The Gysel configuration, which seems to be the most promising one for solid-state high power amplifier combining, has been investigated in theory to derive an exact relationship among its parameters.

Methods for optimizing structures with any number n of ports have been reported.

Measured data on an eight-way PDC, implemented in the DME/TACAN frequency band 960–1215 MHz, are satisfactory for practical purposes.

Though further investigations are required to minimize parasitic reactances, the experimental outcomes can be regarded as being in good agreement with the theoretical ones.

Appendix
Derivation of Impedance Relationships

Substituting (3) into (1) and taking (2) into account results in

$$V_1 = jZ_2\left[\frac{V_a}{Ro} - (n-1)\,j\frac{V_n}{Z_2}\right] \tag{A1}$$

substituting (4) into (2) yields

$$V_a = jZ_2\left[\frac{V_n}{Ro} - I_{nb}\right] \tag{A2}$$

and substituting (4) into (1) results in

$$j\frac{V_a}{Z_2} = \frac{E - V_1}{Ro} - I_{1b}. \tag{A3}$$

In order to express currents I_{1b} and I_{nb} in terms of voltages let us consider a single branch of the internal load subnetwork. From Fig. 7

$$\begin{bmatrix} V_B \\ \dfrac{I_{1c}}{n-1} \end{bmatrix} = \begin{bmatrix} 0 & jZ_4 \\ \dfrac{j}{Z_4} & 0 \end{bmatrix}\begin{bmatrix} 1 & 0 \\ \dfrac{1}{R} & 1 \end{bmatrix}\begin{bmatrix} 0 & jZ_3 \\ \dfrac{j}{Z_3} & 0 \end{bmatrix}\begin{bmatrix} V_n \\ I_{nb} \end{bmatrix}$$

$$= \begin{bmatrix} -\dfrac{Z_4}{Z_3} & -\dfrac{Z_3Z_4}{R} \\ 0 & -\dfrac{Z_3}{Z_4} \end{bmatrix}\begin{bmatrix} V_n \\ I_{nb} \end{bmatrix}. \tag{A4}$$

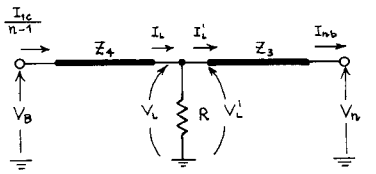

Fig. 7. Internal load subnetwork branch connected at port n.

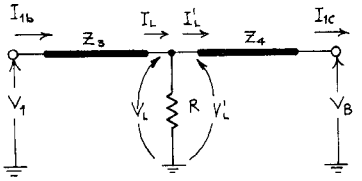

Fig. 8. Internal load subnetwork branch connected at port 1.

On the other hand, from Fig. 8 we derive

$$\begin{bmatrix} V_1 \\ I_{1b} \end{bmatrix} = \begin{bmatrix} -\dfrac{Z_3}{Z_4} & -\dfrac{Z_3Z_4}{R} \\ 0 & -\dfrac{Z_4}{Z_3} \end{bmatrix}\begin{bmatrix} V_B \\ I_{1c} \end{bmatrix}. \tag{A5}$$

Combining (A4) and (A5) we obtain

$$I_{1b} = \frac{n-1}{n}\frac{R}{Z_3^2}(V_1 - V_n) \tag{A6}$$

and

$$I_{nb} = \frac{R}{nZ_3^2}(V_1 - V_n). \tag{A7}$$

Substitution of (A6) and (A7) into (A2) and (A3) results in (5). Setting $V_n = 0$ we get

$$jV_a = \frac{Ro}{Z_2}V_1$$

$$jV_a = \frac{Z_2R}{nZ_3^2}V_1$$

$$E = V_1 + jV_a\frac{Ro}{Z_2} + \frac{n-1}{n}\frac{RRo}{Z_3^2}V_1. \tag{A8}$$

The first two equations imply

$$\frac{Ro}{Z_2} = \frac{Z_2R}{nZ_3^2}. \tag{A9}$$

From the third equation, the perfect matching condition $E/V_1 = 2$ gives

$$\left(\frac{Ro}{Z_2}\right)^2 = 1 - \frac{n-1}{n}\frac{RRo}{Z_3^2}. \tag{A10}$$

Equations (A9) and (A10) can be simultaneously satisfied if and only if

$$\frac{RRo}{Z_3^2} = 1 \tag{A11}$$

$$\left(\frac{Ro}{Z_2}\right)^2 = \frac{1}{n} \tag{A12}$$

from which relationships (8) and (9) follow.

ACKNOWLEDGMENT

The author wishes to thank P. Basile for help with the practical implementation and experimental measurements, and A. Clementi for the review of the manuscript.

REFERENCES

[1] E. J. Wilkinson, "An *N*-way hybrid power divider," *IEEE Trans. Microwave Theory Tech.*, vol. MTT-8, pp. 116–118, Jan. 1960.
[2] K. J. Russell, "Microwave power combining techniques," *IEEE Trans. Microwave Theory Tech.*, vol. MTT-27, pp. 472–478, May 1979.
[3] U. Gysel, "A new *N*-way power divider/combiner suitable for high power applications," in *1975 MTT Symp. Dig.*, pp. 116–118.
[4] *COMPACT™ User Manual*, Version 5.1, Compact Engineering, Palo Alto, CA, Aug. 1979.
[5] H. Howe, Jr., "Simplified design of high power *N*-way, in-phase power divider/combiner," *Microwave J.*, pp. 51–57, Dec. 1979.

An Analytical Investigation of Finlines with Magnetized Ferrite Substrate

Y. HAYASHI AND R. MITTRA, FELLOW, IEEE

***Abstract*—This paper presents an analysis of a unilateral finline printed on a magnetized ferrite substrate. The network analysis method is applied to derive the determinantal equation. Numerical results are presented.**

I. INTRODUCTION

Recently, finlines have become attractive for millimeter-wave integrated-circuit application. Several papers have been published describing experimental and theoretical investigations for the various versions of finline structures printed on dielectric substrates [1]–[7]. Realization of nonreciprocal devices in finline techniques is also of interest in the millimeter-wave range because of the relative compactness and integrability of the devices compared to the nonreciprocal circuits built with conventional ferrite loaded waveguides. Beyer *et al.* [8], [9] have reported the experimental investigations of finline isolators and circulators. The theoretical treatment in [9] is also useful, however, which is based on TE-mode approximation. On the other hand, hybrid-mode analysis methods for the slot and striplines with magnetized ferrite substrates have been reported recently [10]–[12]. Lange [11] and Bock [12] employed the mode-matching procedure, while Mazur *et al.* [10] used the spectral-domain technique, a method which is superior to the former in numerical processing.

This paper presents an analysis method of the finline on a magnetized ferrite substrate. The method is based on the application of the network analysis techniques of electromagnetic fields [13], [14], which is similar to the spectral-domain technique from the viewpoint of applying Fourier transformation. Comparing this theory with the conventional spectral-domain techniques used in [10], however, the equivalent transmission-line concept is ideally suited for the analyses of the planar waveguide structures as indicated in [6], and the modal representation of the fields by TM-to-z, and TE-to-z modes (the z-axis is chosen perpendicular to the boundary surfaces of the substrates) facilitates the derivation of the equations.

Manuscript received July 23, 1982; revised December 17, 1982. This work was supported in part by the Joint Services Electronics Program, N00014-79-C-0424, and in part by the Army Research Office, under Contract DAAG29-82-K-0084.

Y. Hayashi is with the Department of Electrical Engineering and Coordinated Science Laboratory, University of Illinois, Urbana, IL 61801, on leave of absence from the Kitami Institute of Technology, Hokkaido, Japan.

R. Mittra is with the Department of Electrical Engineering and Computer Science Laboratory, University of Illinois, Urbana, IL 61801.

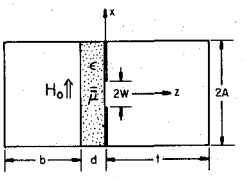

Fig. 1. Cross-sectional view of unilateral finline on ferrite substrate.

The determinantal equation for the propagation constant of a unilateral finline is obtained via matrix formulation in conjunction with Galerkin's procedure. Convergence checks are performed by increasing the number of basis functions for the representation of the aperture field. Some representative numerical results are included in the paper for the frequency range where the effective permeability $\mu_\perp > 0$, while the results for $\mu_\perp < 0$ are shown in [10]. The method is quite general and is applicable to other types of finline structures containing anisotropic media.

II. DETERMINANTAL EQUATION

The unilateral finline to be analyzed here is shown in Fig. 1, where the y-axis is chosen to be the direction of wave propagation. Since the dominant propagating mode of the finline is similar to the TE_{10} mode of the conventional rectangular waveguide, and the H-field near the slot is elliptically polarized, the ferrite slab should be magnetized in a direction parallel to the x-axis to realize efficient nonreciprocal circuits. When a ferrite sample is magnetized to saturation along the x-axis, the dyadic permeability of the ferrite is given by

$$\bar{\bar{\mu}} = \begin{bmatrix} \mu_0 & 0 & 0 \\ 0 & \mu & -jK \\ 0 & jK & \mu \end{bmatrix} \tag{1}$$

where μ_0 is the permeability of free space, and μ and K are dependent on the operating frequency ω, the applied dc magnetic field H_0, and the magnetization of the ferrite $4\pi M_s$.

As a first step toward deriving the determinantal equation, we express $\bar{E}_t$ and $\bar{H}_t$, the fields transverse to the z-axis, via the following Fourier integral:

$$\begin{Bmatrix} \bar{E}_t \\ \bar{H}_t \end{Bmatrix} = \frac{1}{\sqrt{2\pi}} \sum_{l=1}^{2} \sum_{m=0}^{\infty} \cdot \int_{-\infty}^{\infty} \begin{Bmatrix} V_m^{(l)}(\beta:z)\, \bar{f}_m^{(l)}(\beta:x) \\ I_m^{(l)}(\beta:z)\, \bar{g}_m^{(l)}(\beta:x) \end{Bmatrix} e^{-j\beta y_{d\beta}} \tag{2}$$

where $l=1$ and $l=2$ represent the E-waves ($H_z \equiv 0$) and the H-waves ($E_z \equiv 0$), respectively. The vector mode functions $\bar{f}_m^{(l)}$ and $\bar{g}_m^{(l)}$ are given in Appendix I. They satisfy the boundary conditions at $x = \pm A$ and have the following orthonormal properties:

$$\int_{-A}^{A} \bar{f}_m^{(l)} \cdot \bar{f}_{m'}^{(l')*}\, dx = \int_{-A}^{A} \bar{g}_m^{(l)} \cdot \bar{g}_{m'}^{(l')*}\, dx = \delta_{ll'}\delta_{mm'} \tag{3}$$

where $\delta_{kk'}$ is Kronecker's delta, and the asterisk denotes a complex conjugate. Also, in (2) V_m and I_m are the modal voltages and currents. The longitudinal field components are derivable from

0018-9480/83/0600-0495$01.00 ©1983 IEEE